PHYSICAL REVIEW B VOLUME 17, NUMBER 12 15 JUNE 1978

Valence-band structures of III-V compounds and alloys—Bond-orbital and coherent-potential approximations

A.-B. Chen
Auburn University, Auburn, Alabama 36830

A. Sher
College of William and Mary, Williamsburg, Virginia 23185
(Received 13 January 1978)

The bond-orbital model (BOM) and the coherent-potential approximation (CPA) are used to study the valence-band structures of the III-V compound semiconductors GaP, GaAs, GaSb, InP, InAs, and InSb and their alloys. All the third-neighbor bond interactions are included, but the main outstanding defects in the BOM found by previous authors remain. However, the model reproduces the major structure of the observed densities of states. The BOM is especially convenient for alloys because it effectively isolates the important disorder parameters and facilitates the execution of CPA. The model's parameters are deduced by fitting to the photoelectric thresholds and x-ray photoemission spectra. We found that the most interesting CPA results are not the densities of states usually studied but are the more detailed band properties like energy shifts, effective masses, alloy scattering, and optical-absorption-line broadening. This work provides a basic understanding of the effect of alloy disorder on the nonlinear concentration dependence of the energy at the top of the valence band and line broadening of the fundamental optical gap E_0.

I. INTRODUCTION

Because of the importance of semiconductors in science and technology, there have been extensive theoretical and experimental investigations of their electronic structures.[1,2] Consequently, a quantitative understanding of many important parts of the band structures has been deduced. However, the theory of the electronic structure of disordered semiconductors and substitutional alloys is quite rudimentary by comparison. Yet many modern devices function because of the special properties of these alloys, e.g., GaAsP light emitters, GaAs-GaAlAs solar cells, HgCdTe infrared detectors, etc. This motivated our interest in applying a more advanced alloy theory, the coherent-potential approximation[3-5] (CPA), to study the substitutional zinc-blende alloys. This paper contains the results for the valence-band structures of several III-V compound alloys. The techniques used here are readily extended to the conduction bands and to other alloys.

Two theoretical models which have been used frequently to describe the electronic structure in semiconductor alloys are the virtual-crystal approximation[6] (VCA) and the semiempirical dielectric model (DM) of Van Vechten and Bergstresser.[7] Neither of these methods, including perturbation-theory extensions,[8] is sufficiently general to account for the entire range of important band properties that are measurable. On the other hand, CPA is a method that can do so. It is a little surprising that since the pioneering work on the SiGe alloy system by Stroud and Ehrenreich,[9] there has been no major effort to apply CPA to these rather important semiconductor alloy systems. This may be partially a consequence of the level of difficulty and the conclusions drawn in their work. Since CPA calculations involve complicated numerical Brillouin-zone (BZ) integrations, simplifying assumptions were needed to make the calculation tractable. Furthermore, their emphasis was on the alloy density of states, and the potentials of Si and Ge do not differ by enough so the CPA and VCA results have interesting distinctions. However, there are larger potential differences among the III-V and the II-VI compounds. Also, there are physical properties of the systems that are far more sensitive to alloy disorder than the density of states, e.g., the variation with alloy concentration of the band gap, the effective mass, the mobility, etc. In addition to these factors, BZ integration methods have been developed recently[10] that are simple and accurate. Finally, since Stroud and Ehrenreich published their work, considerable progress has been made in the application of the CPA, particularly to metal alloys,[11] hydrides,[12] and phonon spectra.[13] We believe that CPA will prove to be equally useful for semiconductor alloys, especially when it is applied to study properties which are sensitive to disorder.

CPA has been shown to be the best possible "single-site" approximation.[4,5] It not only yields correct results for various limits, e.g., the low-concentration, weak-scattering, and "atomic" limits, but also produces semiquantitative answers in the high-concentration and strong-scat-

tering regimes. The theory also permits a systematic extension beyond its single-site context (i.e., the cluster CPA).[14] However, CPA is easiest to implement when the disorder is localized. In a substitutional semiconductor alloy like $Ga_xIn_{1-x}As$, the cations (i.e., Ga and In) are randomly distributed on one fcc sublattice and each of them is bonded tetrahedrally to four As anions on another fcc sublattice displaced by $(\frac{1}{4}, \frac{1}{4}, \frac{1}{4})a$ relative to the first. The length a is that of the cube edge. Clearly, the most important aspect of disorder in this alloy is the difference between the GaAs and InAs bonds. This disorder can be readily treated in CPA starting from a tight-binding bond-based model referred to as the "bond-orbital model"[15,16](BOM).

The BOM employed here is similar to that used by many previous workers.[16-18] The model reproduces most of the features of the best empirical-pseudopotential band-structure calculations.[2] However, some details are not given properly by the versions of BOM tried to date. In order to examine the possibility of correcting some of the defects noted by previous workers, we have studied the role of the interaction between third-nearest bonds. We shall demonstrate that these higher-order matrix elements do not improve the situation. In particular, even with these interactions included, there is still no dispersion of the bands along the Z axis.

The main advantage of the BOM over other tight-binding basis sets is that its matrix elements of the Hamiltonian divide naturally into large diagonal terms and smaller off-diagonal terms. This facilitates approximations and allows identification of the important terms. To gain some insight into the variation of the BOM parameters from one material to another, we parametrize them for six III-V compounds in three different ways. We found that the large diagonal bond energies have moderately large systematic variations from one compound to another for all three fitting methods. However, the smaller off-diagonal matrix elements varied by much smaller amounts and the changes are not systematic. Consequently, the off-diagonal elements are treated in VCA, while CPA is reserved for the diagonal elements. This simplifies the analysis greatly. This study also emphasizes the need to determine the parameters from a common experimental source. For this purpose, our BOM parameters were finally determined by fitting the broadened density of states to the x-ray valence-band spectra measured by Ley *et al.*[19]

When disorder in the bond energies is treated in CPA and other parameters are assigned according to VCA, the 4×4 matrix equation for the CPA self-energy reduces to a scalar equation. The only Brillouin-zone integration arises in the calculation of the VCA Green's function. A straightforward iteration procedure[20] leads to a rapidly converging solution. Similar to the previous CPA result for the SiGe alloy,[9] our result[21] for the III-V compound alloys shows that the CPA density of states merely represents an uninteresting smoothing of the VCA result even for the strongest-scattering case among the six alloys studied. The smoothing is characterized as uninteresting because its effects lie just outside the resolution limits of current experiments. As the experiments improve, this extra smoothing could become interesting. However, as noted above, CPA results that can be compared against experiments do arise. One interesting example is the concentration variation of the energy levels. CPA predicts a positive bowing parameter for the fundamental gap E_0.[22] The CPA calculation also predicts that the broadening of the levels at the top of the valence band will be quite small, which again is consistent with the lack of alloy broadening in the observed E_0 spectra.[22,23] These results help to resolve some questions about the effect of disorder on the gap variation in semiconductor alloys.[21]

The rest of the paper is arranged in the following order. In Sec. II, the BOM is defined, including the expressions for the matrix elements and the band energies along the symmetry axis. In Sec. III, the procedures for determining the BOM parameters and the effects of truncation are discussed. In Sec. IV, a comparative study of the BOM parameters determined from three different experiments is made, and the best of these, a fit of the broadened BOM density of states to the x-ray valence-band spectra for six III-V compounds, is presented in detail. The combined CPA-BOM calculation is formulated in Sec. V. The results for the III-V compound alloys are presented and discussed in Sec. VI. The conclusions are summarized in Sec. VIII, and extensions to this project are suggested.

II. BOND-ORBITAL MODEL

A semiconductor with a zinc-blende structure such as GaAs consists of two sublattices, the anion (i.e., As) and the cation (Ga) sublattices, which are displaced from each other by a vector $\vec{\tau}=(\frac{1}{4}, \frac{1}{4}, \frac{1}{4})a$, where a is the lattice constant. Consequently, each anion in the crystal is surrounded by a tetrahedral arrangement of four cations and vice versa. A schematic picture of a flattened network of the structure is shown in Fig. 1. The recent work by Harrison and his co-workers[15]

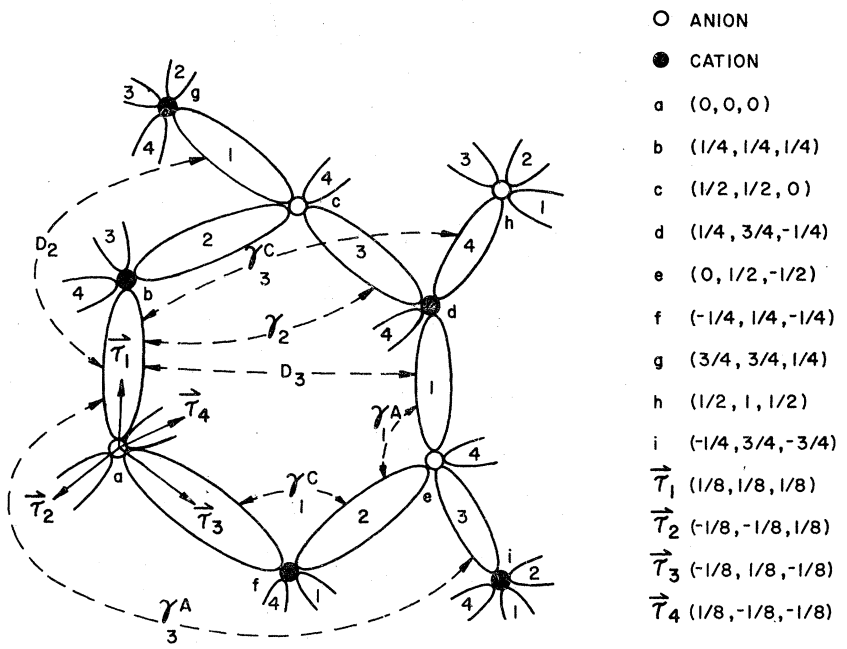

FIG. 1. Schematic flattened diagram for zinc-blende crystals. The open circles represent the anions and the dots represent the cations. Each atom is surrounded by four bonds. The centers of the bonds are specified by four vectors $\vec{\tau}_1$, $\vec{\tau}_2$, $\vec{\tau}_3$, and $\vec{\tau}_4$ from each anion. The location of the atoms in the diagram are labeled with lower-case letters. The coordinates and the vectors are in units of the lattice constant a. The interactions between bonds are also indicated in the diagram.

has demonstrated that the systematics of the bonding and various physical properties can be reasonably described by a simple molecular model referred to as the "bond-orbital model." In this model, the basis functions are centered on bonds connecting each anion and the nearest cations. These basis functions are constructed from the combination of the sp^3 hybrides of the two atoms adjacent to the bond that diagonalize the local Hamiltonian.[24] This construction results in bonding and antibonding orbitals. In the bond-orbital approximation for the valence bands, the antibonding states are discarded, and Bloch states are formed from linear combinations of the bonding states only. The earlier work by Stoker,[18] and the more recent studies by Shevchik, Tejida, and Cardona,[17] and by Pantelides and Harrison[16] produced BOM predictions for most of the interesting semiconductor electronic properties including the density of states,[17] the expressions for the various matrix elements, and the band energies. While the bands agree with other results in many important structures, there are some defects associated with the model. The most noticeable defects, which directly affect the density of states, are a missing dip in the upper Σ_1 band and the lack of dispersion for the bands along the Z axis.[16,17,25]

Based on the results of the tight-binding band structures by Chadi and Cohen,[26] Pantelides[25] speculated that these defects were caused by the omission of the anion-anion interaction in the BOM calculations. As a consequence, we have included all the third-nearest-neighbor bond interactions to see if these extra matrix elements would lead to a better starting point for the alloy study. Since the effects of these matrix elements have not been discussed in the literature and since they will be used later in the alloy study, we shall next treat them explicitly.

We begin by establishing the BOM basis set and our notation. We use one of the fcc sublattices (for definiteness the anion sublattice) as the reference lattice in which each lattice point is represented by a lattice vector $\vec{j}$. Then each point $\vec{j}$ is surrounded by four bond orbitals $\{|\vec{j}\,\alpha\rangle\}$ centered at the four displacements $\vec{j}+\vec{\tau}_\alpha(\alpha=1,2,3,4)$, where $\vec{\tau}_1=(\frac{1}{8},\frac{1}{8},\frac{1}{8})a$, $\vec{\tau}_2=(-\frac{1}{8},-\frac{1}{8},\frac{1}{8})a$, $\vec{\tau}_3=(-\frac{1}{8},\frac{1}{8},-\frac{1}{8})a$, and $\vec{\tau}_4=(\frac{1}{8},-\frac{1}{8},-\frac{1}{8})a$ (see Fig. 1). Here we assume that the orbitals $\{|\vec{j}\,\alpha\rangle\}$ are Wannier-type orbitals so they are orthonormal $\langle\vec{j}\alpha|\vec{j}'\alpha'\rangle=\delta_{\vec{j}\vec{j}'}\delta_{\alpha\alpha'}$. In fact, the bond orbitals are not orthogonal, but most of the effect of nonorthogonality can be absorbed into the parametrizations.[15] When expanded in terms of the bond basis set $\{|\vec{j},\alpha\rangle\}$, the BOM Hamiltonian takes the form

$$H_0=\sum_{\vec{j}\alpha\vec{j}'\alpha'}|\vec{j}\alpha\rangle\langle\vec{j}\alpha|H_0|\vec{j}'\alpha'\rangle\langle\vec{j}'\alpha'|\,.$$

If the bond-to-bond transition interactions are truncated at the third nearest-neighbor bonds, there are eight distinct interactions $\langle\vec{j}\alpha|H_0|\vec{j}'\alpha'\rangle$ which are defined below (also see Fig. 1):

D: (the bond energy)$\langle\vec{j}\alpha|H_0|\vec{j}\alpha\rangle$

γ_1^A: the matrix elements between adjacent bonds with an anion in common,

γ_1^C: the matrix element between adjacent bonds with a cation in common,

D_2: the matrix element between parallel second-nearest bonds, i.e., $\langle\vec{j}\alpha|H_0|\vec{0}\alpha\rangle$ with $|\vec{j}|=a/\sqrt{2}$,

γ_2: the matrix element between nonparallel second-nearest bonds,

D_3: the matrix element between parallel third-nearest bonds,

γ_3^A: matrix elements between nonparallel third-nearest bonds with the closer ends adjacent to anions,

γ_3^C: matrix elements between nonparallel third-nearest bonds with the closer ends adjacent to cations.

For later convenience, we further define the symmetric matrix elements

$$\gamma_1^s\equiv\tfrac{1}{2}(\gamma_1^A+\gamma_1^C)\text{ and }\gamma_3^s\equiv\tfrac{1}{2}(\gamma_3^A+\gamma_3^C)\,,$$

and the antisymmetric ones

$$\gamma_1^a\equiv\tfrac{1}{2}(\gamma_1^A-\gamma_1^C)\text{ and }\gamma_3^a\equiv\tfrac{1}{2}(\gamma_3^A-\gamma_3^C)\,.$$

The corresponding Bloch basis functions can be constructed from the bond orbitals by

$$|\vec{k}\alpha\rangle\equiv\frac{1}{\sqrt{N}}\sum_{\vec{j}}e^{i\vec{k}\cdot(\vec{j}+\vec{\tau}_\alpha)}|\vec{j}\alpha\rangle\,,\qquad(1)$$

where N is the total number of anions or cations in the crystal and $\vec{k}$ is a wave vector in the Brillouin zone. These Bloch functions are also orthonormal, i.e., $\langle\vec{k}\alpha|\vec{k}'\alpha'\rangle=\delta_{\vec{k}\vec{k}'}\delta_{\alpha\alpha'}$, but they are not the eigenfunctions of H_0. The matrix elements of H_0 in terms of these Bloch basis functions are related to the interbond interactions by the expression

$$\langle\vec{k}\alpha|H_0|\vec{k}'\alpha'\rangle=\delta_{\vec{k}\vec{k}'}\sum_{\vec{j}}e^{-i\vec{k}\cdot(\vec{j}+\vec{\tau}_\alpha-\vec{\tau}_{\alpha'})}\times\langle\vec{j}\alpha|H_0|\vec{0}\alpha'\rangle\,.\qquad(2)$$

The explicit expressions, with the full third-nearest bond interactions included, for these matrix elements and for the band energies along the Δ and Λ axes are given in Appendix A. From these expressions we can write the energies at the symmetry points Γ, X, and L. These energies are:

$$\Gamma_{15}=D+6D_2+6D_3-2\gamma_1^s-4\gamma_2-14\gamma_3^s\qquad(3a)$$

which is threefold degenerate,

$$\Gamma_1=D+6D_2+6D_3+6\gamma_1^s+12\gamma_2+42\gamma_3^s\,,\qquad(3b)$$

$$X_5=D-2D_2-2D_3-2\gamma_1^s+4\gamma_2+2\gamma_3^s\qquad(3c)$$

which is twofold degenerate,

$$X_{3,1}=D-2D_2-2D_3+2\gamma_1^s-4\gamma_2-2\gamma_3^s\mp2(2\gamma_1^a+6\gamma_3^a)\,,\qquad(3d)$$

$$L_3=D+2D_2-2D_3-2\gamma_1^s+2\gamma_3^s\qquad(3e)$$

which is twofold degenerate, and

$$L_{2,1}=D-2D_2+2D_3+2\gamma_1^s-2\gamma_3^s\pm2[(2D_2-2D_3+\gamma_1^s-\gamma_3^s)^2+3(\gamma_1^a-\gamma_3^a)^2]^{1/2}\,.\qquad(3f)$$

We note that, besides having more terms, the above expressions differ in another way from the corresponding equations in the previous work.[16] Usually, the top of the valence band (i.e., Γ_{15}) was used as the reference level, i.e., $\Gamma_{15}=0$. This choice is, of course, not suitable for the alloy problem since the Γ_{15} level varies from compound to compound. Thus, the parameters and the energies that we have discussed so far are all referred to the vacuum level.

III. PARAMETRIZATION OF THE INTERACTIONS AND THE EFFECT OF TRUNCATION

As studies on metals[27] and semiconductors[2] have shown, the only practical means for obtaining quantitatively accurate band structures is to incorporate some experimental data into the calculation. This is especially true in these alloy studies where the objective is a practical theory to correlate with a wide range of experiments. Thus, we shall also adopt the empirical parametrization approach. To facilitate the parametrizations, it is convenient to express the BOM matrix elements in terms of the following energy separations:

$$D_2-\gamma_2=\tfrac{1}{4}(L_3-X_5)\equiv\delta_1\,,\qquad(4a)$$

$$\gamma_1^s-2\gamma_2-\gamma_3^s=\tfrac{1}{8}(X_1+X_3-2X_5)\equiv\delta_2\,,\qquad(4b)$$

$$D_2-D_3-\gamma_1^s+\gamma_3^s=\tfrac{1}{8}(2L_3-L_2-L_1)\equiv\delta_3\,,\qquad(4c)$$

$$D_2+D_3-\gamma_2-3\gamma_3^s=\tfrac{1}{8}(\Gamma_{15}-X_5)\equiv\delta_4\,,\qquad(4d)$$

$$\gamma_1^s+2\gamma_2+7\gamma_3^s=\tfrac{1}{8}(\Gamma_1-\Gamma_{15})\equiv\delta_5\,,\qquad(4e)$$

$$\gamma_1^a+3\gamma_3^a=\tfrac{1}{8}(X_1-X_3)\equiv\delta_6\,,\qquad(4f)$$

$$[(2D_2-2D_3+\gamma_1^s-\gamma_3^s)^2+3(\gamma_1^a-\gamma_3^a)^2]^{1/2}=\tfrac{1}{4}(L_2-L_1)\equiv\delta_7\,.\qquad(4g)$$

Note that except for D, which measures the center of gravity of the bands, all seven of the other parameters needed for the band structures are contained in the above equations. The determina-

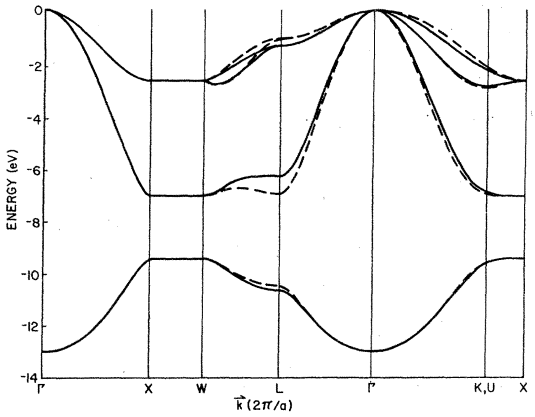

FIG. 2. Comparison of the bands calculated without third-neighboring interactions (the solid curves) and those found including D_3 (the dashed curve).

tion of D will be discussed later.

It should be mentioned that in order to produce dispersion of the Δ_5 bands and of the Λ_3 bands (see Fig. 2), at least the second-nearest bond parameters D_2 and γ_2 have to be included.[16,17] The numerical results of Pantelides and Harrison[16] were based on the truncation in which $D_3 = \gamma_3^s = \gamma_3^a = 0$. Then, the above equations yield the four parameters

$$\gamma_1^s = \tfrac{1}{2}(\delta_2 + \delta_5), \tag{5a}$$

$$\gamma_1^a = \delta_6, \tag{5b}$$

$$\gamma_2 = \tfrac{1}{4}(\delta_5 - \delta_2), \tag{5c}$$

$$D_2 = \tfrac{1}{4}(\delta_5 - \delta_2) + \delta_4, \tag{5d}$$

plus two sum rules $\delta_1 = \delta_4$ and $\delta_5 - 3\delta_4 - 4(\delta_3 - \delta_4) = 0$. If D_3 is added, γ_1^s, γ_1^a, and γ_2 are still given by Eqs. (5a)–(5c), respectively, but D_2 and D_3 become

$$D_2 = \delta_1 + \tfrac{1}{4}(\delta_5 - \delta_2), \tag{6a}$$

$$D_3 = \delta_4 - \delta_1, \tag{6b}$$

and a new sum rules results

$$4\delta_1 - 3\delta_2 - 4\delta_3 - 4\delta_4 + \delta_5 = 0. \tag{7}$$

The four parameters in Eqs. (5a)–(5d) only determine the energy levels Γ_1, X_5, X_3, X_1 with respect to the Γ_{15} level. The addition of the D_3 parameter also fixes the L_3 level. Figure 2 shows a comparison between the bands resulting from these two different procedures, the first includes D_3 (the dashed curves) and the other (the solid curves) has $D_3 = 0$. The bands along the ⟨100⟩ axis (i.e., the Δ axis) derived from both procedures are identical, but those going from Γ in other directions are different, particularly those along the Λ direction. Three outstanding defects (see Fig. 2) in the BOM band structures have been pointed out by previous workers: (a) the top bands at Γ are too flat[16] (have effective masses at Γ_{15} that are too large), (b) compared to more elaborate calculations the dip in the upper Σ_1 band (the second band from the top along the K direction) is not deep enough,[25,26] and (c) more striking, there is no dispersion along the Z direction (from X to W).[25,26] From Fig. 2, it is evident that the inclusion of D_3 does not correct these defects. However, D_3 does help to pin down the L_3 level.

The next question is whether the inclusion of γ_3^s and γ_3^a would improve the situation. Note first that not all seven equations in Eqs. (1) are independent. The sum rule in Eq. (7) still holds even when γ_3^s and γ_3^a are included. This means that the whole set of parameters cannot be determined without additional information. However, we can understand the effects of these parameters without actually carrying out the parametrization. First, examine the effective masses. The dispersion for the Δ_5 band has the general form [see Eq. (A1) in Appendix A] $A + B\cos 2x$, and the Λ_3 band has the form $A' + B'\cos 4x$ [Eq. (A3)]. This means that the coefficients A, B, A', and B' and, thus, the effective masses at Γ_{15} are fixed once the two ends of the bands are fitted. Hence, no improvement in the effective masses is possible within the context of the present model. Also, the bands along the Z axis remain flat even when γ_3^s and γ_3^a are included. An analytic proof of this result is given in Appendix B. Numerical experiments, with the expression $\gamma_1^a/\gamma_1^s = \gamma_3^a/\gamma_3^s$ used to close the set of equations, show that the dip in the Σ_1 direction is not affected much by γ_3^s, γ_3^a. These results show that the inclusion of γ_3^s and γ_3^a do not help to correct the remaining defects of the BOM. Therefore, in the rest of this work, we shall use the BOM with $\gamma_3^s = \gamma_3^a = 0$ but with all the other parameters defined in Sec. I included.

IV. EMPIRICAL BOM PARAMETERS

Now that the model is established, we can obtain the parameters from any set of band energies by using the algebraic equations (5a)–(6b). A systematic parametrization has been carried out for six III-V compounds: GaP, GaAs, GaSb, InP, InAs, and InSb. Three sets of band structure results were studied. They are (i) the nonlocal pseudopotential calculation by Chelikowsky and Cohen,[2] (ii) the valence-band energies determined from the x-ray photoemission work by Ley *et al.*,[19] and (iii) the band energies derived from the uv photoemission spectra by Eastman *et al.*[28] Table I lists the input energies (relative to Γ_{15}) and the corresponding parameters except for D.

TABLE I. Input band energies (in eV with respect to Γ_{15}) and the parameters based on Eqs. (5a) to (6b). The labels (b), (c), and (d) refer to the input energies, Refs. 2, 19, and 28, respectively.

		Γ_1	X_5	X_3	X_1	L_3	D_2	D_3	γ_1^s	γ_1^a	γ_2
GaP	(b)	−13.0	−2.7	−7.1	−9.5	−1.1	0.3437	−0.0625	−1.5125	−0.3000	−0.0563
	(c)	−13.2	−2.7	−6.9	−9.6	−1.2	0.3094	−0.0375	−1.5187	−0.3375	−0.0656
	(d)	−11.8	−2.7 [a]	−6.9	−9.7	−0.8	0.4562	−0.1375	−1.4375	−0.3500	−0.0188
GaAs	(b)	−12.1	−2.9	−6.9	−9.9	−1.3	0.3656	−0.0375	−1.4437	−0.3750	−0.0344
	(c)	−13.8	−2.5	−7.1	−10.7	−1.4	0.2437	0.0375	−1.6625	−0.4500	−0.0313
	(d)	−12.9	−2.9 [a]	−6.9	−10.0	−0.8	0.4687	−0.1625	−1.5000	−0.3875	−0.0563
GaSb	(b)	−12.0	−2.5	−6.8	−9.3	−1.2	0.2969	−0.0125	−1.4437	−0.3125	−0.0219
	(c)	−11.6	−2.7	−6.9	−9.4	−1.3	0.3281	−0.0125	−1.4062	−0.3125	−0.0219
InP	(b)	−11.3	−2.0	−5.9	−8.8	−0.9	0.2562	−0.0250	−1.3750	−0.3625	−0.0187
	(c)	−11.0	−2.0	−5.9	−8.9	−1.0	0.2437	0.0	−1.3625	−0.3750	−0.0063
InAs	(b)	−12.5	−2.2	−6.4	−10.0	−0.9	0.3094	−0.0500	−1.5312	−0.4500	−0.0156
	(c)	−12.3	−2.4	−6.3	−9.8	−0.9	0.3437	−0.0750	−1.4750	−0.4375	−0.0313
InSb	(b)	−11.3	−1.9	−6.0	−8.8	−0.8	0.2656	−0.0375	−1.3937	−0.3500	−0.0094
	(c)	−11.7	−2.4	−6.4	−9.5	−1.4	0.2313	0.0500	−1.4250	−0.3870	−0.0187
	(d)	−11.2	−1.9 [a]	−6.5	−9.0	−1.05	0.2281	0.0250	−1.4312	−0.3125	0.0156

[a] These numbers were not available from the original source. We used the same values as those in (b).

[The values for $D-\Gamma_{15}$ can be obtained from Eq. (9)]. Several general results can be observed.

(i) The size of the matrix elements for a given compound decreases very rapidly as the separation between the connected bonds increases. For example, D_3 is about one order of magnitude smaller than D_2 and γ_2 is only about 1% to 3% of γ_1^s.

(ii) The variation of the more important larger hopping matrix elements D_2, γ_1^s, and γ_1^a from one compound to another is fairly small and not very systematic.

(iii) The variation of these parameters for the same compound using different sets of band-structure data is at least as large as that between different compounds.

(iv) The smaller parameters γ_2 and D_3 seem to vary in a random fashion. These observations not only provide some justification for using the CPA alloy model to be discussed later but also indicate the importance of determining the parameters for alloy calculations by fitting to a consistent data set.

The experimental data of Ley *et al.*[19] furnish a suitably consistent starting point. Their data include all six of the Ga and In compounds treated here. However, if we simply start from the symmetry point energies given in their Table I, the resulting BOM densities of states do not fit their major peaks. This occurs because their energies were based on a fit to a more sophisticated band structure. Consequently, we have refit directly to their data by adjusting the parameters so that the peaks of the calculated broadened density of states agree with the positions of the experimental peaks.

The density of states can be calculated efficiently by using a simple Brillouin-zone integration method recently developed by one of us.[9] The unbroadened densities of states $\rho_0(E)$ for the six compounds studied are given by the short dashed curves in Figs. 3(a)–3(f), while the broadened $\rho(E)$ are given by the solid curves. The broadening was carried out by a convolution of $\rho_0(E)$ with a Lorentzian of width $\Gamma(E)$:

$$\rho(E)=\frac{1}{\pi}\int_{-\infty}^{\infty}\frac{\Gamma(E')}{\Gamma^2(E')+(E-E')^2}\rho_0(E')\,dE' . \tag{8}$$

A linearly varying $\Gamma(E)$ was used which starts with a value of 0.35 eV at the highest energy and ends with a value of 0.5 eV at the lowest energy shown in the figures. Also in Figs. 3(a)–3(f), the experimental spectra by Ley *et al.*, the long dashed curves, are shown for comparison. The peak positions are accurately reproduced; the line shapes for the lower two peaks are also approximately correct, but the distinct low-energy shoulders in the experimental curves on the top peaks are missing in the theoretical curves because of the defects of BOM mentioned earlier.

The energies at Γ, X, and L, and the corresponding bond parameters are tabulated in Table II. Most of these values are close to the corresponding values in Table I, but there are some differences. The parameters in Table II will be

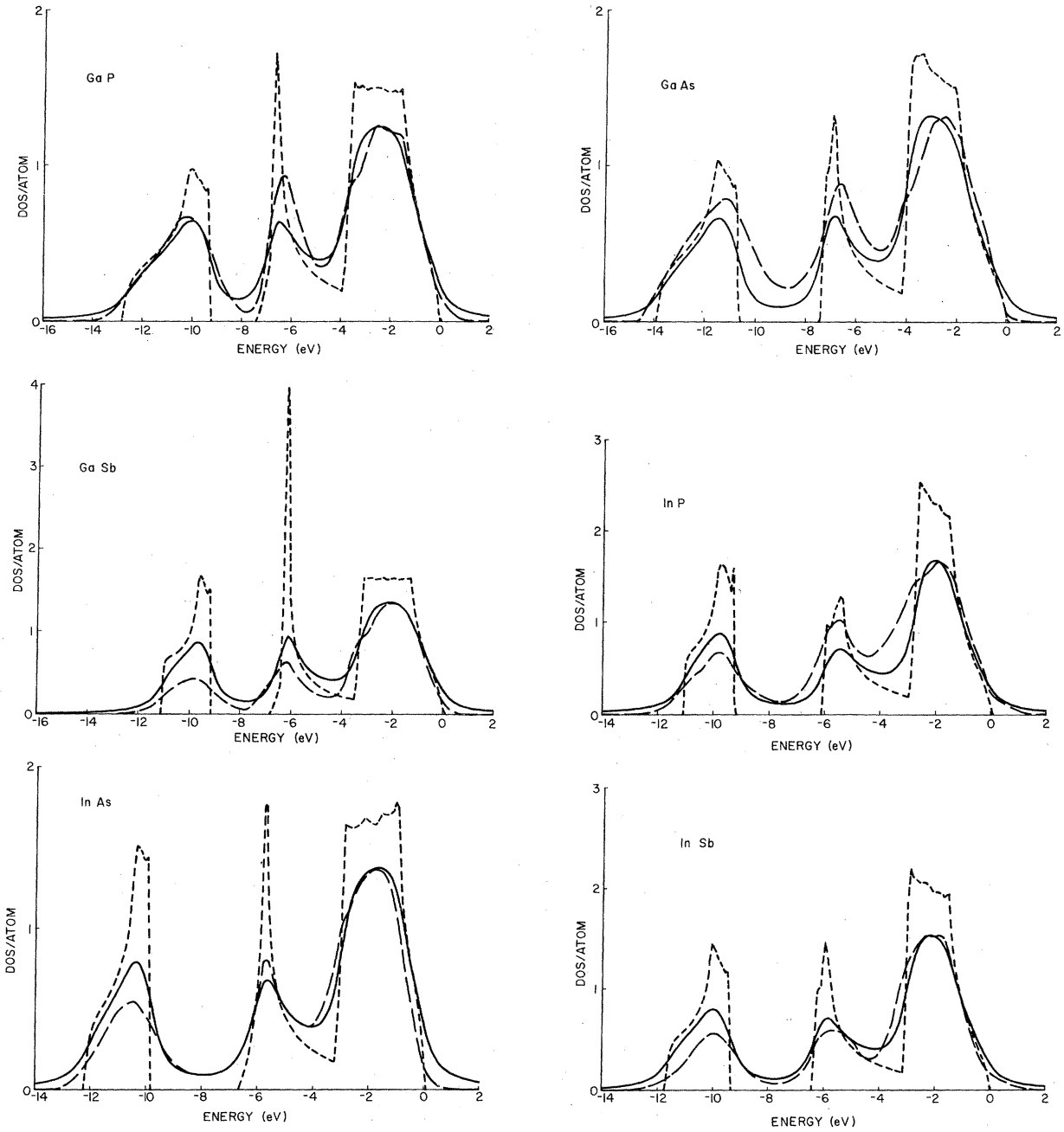

FIG. 3. Comparison of the broadened theoretical density of states (the solid curves) and the experimental x-ray valence-band spectra (the long dashed curves) in Ref. 19 for six compounds. The unbroadened densities of states (the short dashed curves) are also shown.

used later in the alloy study.

Finally, we turn to the question of determining the bond-energy parameter D. From Eqs. (3a)–(3d), the difference $D-\Gamma_{15}$ can be shown to depend only on symmetry-point energy separations,

$$D-\Gamma_{15}=\tfrac{3}{16}(X_1+X_3-2X_5)+\tfrac{3}{4}(X_5-\Gamma_{15})+\tfrac{1}{16}(\Gamma_1-\Gamma_{15}), \quad (9)$$

and is independent of the truncations discussed in Sec. III. Thus, D can be determined empirically using the band energies in Table II and the experimental values of the photoelectric thresholds. The values of $D-\Gamma_{15}$ are listed in Table III along with the thresholds measured by Shevchik *et al.*[29] and the values of D. The thresholds used here agree with previous measurements[30] to within 0.05 eV.

TABLE II. Band energies (in eV) with respect to the top of the valence band and the intrabond matrix elements (also in eV) corresponding to the fitted valence-band densities of states shown in Figs. 3(a)–3(f).

	GaP	GaAs	GaSb	InP	InAs	InSb
Γ_1	−12.8	−13.9	−11.1	−11.1	−12.2	−11.7
X_5	−3.5	−3.8	−3.1	−2.7	−2.8	−2.9
X_3	−6.7	−7.3	−6.2	−6.0	−5.8	−6.3
X_1	−9.3	−10.7	−9.2	−9.3	−9.9	−9.4
L_3	−1.5	−2.0	−1.3	−1.5	−1.0	−1.5
L_2	−7.3	−7.0	−6.7	−5.4	−6.5	−6.0
L_1	−10.2	−11.6	−9.7	−9.9	−10.5	−10.1
D_2	0.3812	0.3406	0.3906	0.2625	0.3844	0.2937
D_3	−0.0625	0.0250	−0.0625	0.0375	−0.0100	0.0125
γ_1^s	−1.3625	−1.5187	−1.2687	−1.3125	−1.3937	−1.3500
γ_1^a	−0.3250	−0.4250	−0.3750	−0.4125	−0.5125	−0.3875
γ_2	−0.1188	−0.1094	−0.0594	−0.0375	−0.0656	−0.0563

We see that the energy differences among the D values are large compared to those among the parameters in Table II. We note that a measure of the alloy scattering strength is the ratio of difference between the interaction parameters of the constituent compounds to the average bandwidth (which is of order of 10 eV in our case). If these numbers are very small, VCA is a good approximation. The above results show that the diagonal bond energies D are the only ones for which CPA will differ appreciably from VCA.

V. ALLOY MODEL

In this section, we shall define the BOM Hamiltonian for the III-V compound alloys and develop the necessary CPA formalism. The numerical methods required to implement evaluations of the CPA equation will also be discussed. The numerical results obtained in the previous section will guide our definition of the alloy model. Because the parameters in Table I do not vary systematically, and the uncertainties in the parameters are as large as the variations among the different compounds, it would be inappropriate in this early stage of the development to attempt to treat these parameters beyond the virtual-crystal approximation. However, as noted before, the differences between these parameters for any two compounds is small compared to the bandwidths, so VCA is a good first approximation in any case. There is still another reason for this choice. The present model, on one hand, properly treats the major effects, yet remains simple enough to be handled efficiently. The parameters in Tables I and II are off-diagonal in the bond basis and the treatment of this kind of off-diagonal randomness[31–33] would involve considerable extra complications.

On the other hand, the bond-diagonal parameter D has a larger variation from one compound to another and the procedure for obtaining this parameter [see Eq. (9) and Table III] is well defined. Thus, our alloy Hamiltonian takes the form

$$H_{\text{alloy}} = \overline{H} + \sum_{\vec{l}} V_{\vec{l}} , \tag{10}$$

TABLE III. Values of $D - \Gamma_{15}$ from Eq. (9), the photoelectric thresholds from Ref. 29 and the resulting bond energies (all in eV) for six III-V compounds.

	GaP	GaAs	GaSb	InP	InAs	InSb
$D - \Gamma_{15}$	−5.1125	−5.6687	−4.7437	−4.5750	−4.7562	−4.7625
thresholds	5.7	5.5	4.9	5.7	5.3	4.8
D	−10.8125	−11.1687	−9.6437	−10.2750	−10.0562	−9.5625

where $\overline{H}$ is the BOM Hamiltonian in VCA, and the indices $\vec{j}$ are the lattice vectors that locate the substitutional atoms on their sublattice sites. We shall refer to these randomly distributed atoms on one sublattice as A and B with fractional concentrations x and $1-x$, respectively. The random potential can then be written

$$V_{\vec{j}} \equiv \sum_{\alpha=1}^{4} |\vec{j}\alpha\rangle (D_{\vec{j}} - \overline{D}) \langle \vec{j}\alpha| , \tag{11}$$

where $D_{\vec{j}}$ takes the value D_A if an A atom is located at $\vec{j}$, and D_B if a B atom is at $\vec{j}$, and $\overline{D}$ is the VCA bond energy parameter in $\overline{H}$.

In the CPA formalism, the configuration-averaged one-electron Green's function $\langle G(z)\rangle$ is replaced by an effective Green's function $G_{\text{eff}} \equiv (z - H_{\text{eff}})^{-1}$, where the effective Hamiltonian has the form

$$H_{\text{eff}} = \overline{H} + \sum_{\vec{j}} \Sigma_{\vec{j}} \tag{12}$$

with the self-energy $\Sigma_{\vec{j}}$ satisfying the self-consistent condition $\langle t_{\vec{j}} \rangle = 0$, where the atomic t matrix is

$$t_{\vec{j}} \equiv (V_{\vec{j}} - \Sigma_{\vec{j}})[1 - G_{\text{eff}} (V_{\vec{j}} - \Sigma_{\vec{j}})]^{-1} . \tag{13}$$

We can understand the more detailed structure of Eq. (13) by thinking of the operators as matrices in the basis set $\{|\vec{j}\alpha\rangle\}$. The self-energy is block diagonal with each block identified by a $\vec{j}$. Moreover, each block has the identical 4×4 matrix structure

$$\vec{\vec{\Sigma}} = \begin{bmatrix} \sigma & \lambda & \lambda & \lambda \\ \lambda & \sigma & \lambda & \lambda \\ \lambda & \lambda & \sigma & \lambda \\ \lambda & \lambda & \lambda & \sigma \end{bmatrix} . \tag{14}$$

Thus, in the matrix representation, Eq. (13) can be cast into the form

$$\vec{\vec{\Sigma}} = -[(D_A - \overline{D})\vec{\vec{1}} - \vec{\vec{\Sigma}}] \cdot \vec{\vec{F}} \cdot [(D_B - \overline{D})\vec{\vec{1}} - \vec{\vec{\Sigma}}] , \tag{15}$$

where $\vec{\vec{F}}$ has the matrix elements

$$F_{\alpha\beta}(z) \equiv \langle \vec{j}\alpha | G_{\text{eff}} | \vec{j}\beta \rangle = \frac{1}{N} \sum_{\vec{k}} e^{i\vec{k}\cdot(\vec{\tau}_\alpha - \vec{\tau}_\beta)} \times g_{\alpha\beta}(\vec{k}, z) , \tag{16}$$

with

$$g_{\alpha\beta}(\vec{k}, z) \equiv [z - H_{\text{eff}}(\vec{k})]^{-1}_{\alpha\beta} . \tag{17}$$

The matrix element $[H_{\text{eff}}(\vec{k})]$ is similar to $H_{\alpha\beta}(\vec{k})$ defined in Appendix A except that D is replaced by $\overline{D} + \sigma$ and either γ_1^A is replaced by $\overline{\gamma}_1^A + \lambda$ or γ_1^c by $\overline{\gamma}_1^c + \lambda$ depending on whether the random atoms are anions or cations.

The numerical solution for λ and σ in Eq. (15) encounters the BZ integrations [Eq. (16)], which for an extensive study is quite costly to compute even though we are equipped with a powerful BZ method.[9] However, the effect of a nonvanishing λ is to modify the effective hopping among bonds adjacent to the random sites. From the numerical results of Sec. IV, we have just concluded that at this stage, we should not treat these interactions beyond VCA. Furthermore, the size of λ is only a small fraction of σ because $|\lambda/\sigma|$ is scaled by the ratio $|F_{\alpha\alpha}/F_{\alpha\beta}|$ which is small. This can be understood from Eq. (16) where the phase factor $\exp[i\vec{k}\cdot(\vec{\tau}_\alpha - \vec{\tau}_\beta)]$ for $\alpha \neq \beta$ will result in some cancellation in the BZ integrations. Numerical evidence supporting this argument can be found in the work of Wolfram and Callaway[34] for simple-cubic crystals. Thus we expect that to the same level of approximation as our alloy model [Eq. 10] we can take

$$\Sigma_{\vec{j}} \cong \sum_{\alpha} |\vec{j}\alpha\rangle \sigma \langle \vec{j}\alpha| . \tag{18}$$

This result can also be obtained if one assumes that each bond is an independent scattering center and the "single-bond" CPA is applied to our model. We shall adopt Eq. (18) for our later discussion.

A consequence of Eq. (18) is a tremendous reduction of the formidable BZ integrations. Eq. (15) now reduces to a scalar equation

$$\sigma = -(D_A - \overline{D} - \sigma) f(z-\sigma)(D_B - \overline{D} - \sigma) , \tag{19}$$

where

$$\begin{aligned} f(z-\sigma) &\equiv \langle \vec{j}\alpha | G_{\text{eff}} | \vec{j}\alpha \rangle \\ &= \frac{1}{4} \sum_{\alpha=1}^{4} \langle \vec{j}\alpha | G_{\text{eff}} | \vec{j}\alpha \rangle \\ &= \frac{1}{4N} \sum_{\vec{j}\alpha} \langle \vec{j}\alpha | G_{\text{eff}} | \vec{j}\alpha \rangle \\ &= \frac{1}{4N} \operatorname{Tr} G_{\text{eff}} \\ &= \frac{1}{4N} \sum_{n\vec{k}} \frac{1}{z - \sigma - \epsilon_n(\vec{k})} \\ &= \frac{1}{4N} \left(\frac{\Omega}{N}\right) \frac{1}{(2\pi)^3} \sum_n \int_{\text{BZ}} d^3k \, \frac{1}{z - \sigma - \epsilon_n(\vec{k})} \\ &= \frac{1}{4\pi} \int d\epsilon \, \frac{1}{z - \sigma - \epsilon} \\ &\qquad \times \left[\frac{\Omega}{N} \frac{1}{(2\pi)^3} \sum_n \int d^3k \, \delta(\epsilon - \epsilon_n(\vec{k})) \right] \\ &= \frac{1}{4} \int d\epsilon \, \frac{\overline{\rho}(\epsilon)}{z - \sigma - \epsilon} \end{aligned} \tag{20}$$

and $\bar{\rho}(\epsilon)$ is the VCA density of states per unit cell. Thus, the CPA equation becomes very easy to evaluate once $\bar{\rho}(\epsilon)$ is calculated. The iteration procedure[20] based on the average-t-matrix (ATA) equation will be used to solve Eq. (19).

Before discussing the numerical results, we should point out that the parameters in the VCA $\overline{H}$ can have different forms depending on which averaging procedure is used.[7,23] The simplest procedure is a straightforward average, i.e., $\overline{H} = xH_A + yH_B$, of the two Hamiltonians for the pure constituent compounds. This averaging procedure yields band energies with a linear concentration dependence. However, more elaborate averaging procedures could be adopted. These procedures are intended to account for renormalization of the potentials in the alloy that occur because of charge shifts in the disordered system and changes in the lattice parameter. These effects will introduce nonlinear concentration dependences[7,23] into the energies even in VCA. The matrix elements probably will not be just simple mean values or even quantities rigidly scaled by a simple power law of the lattice spacing.[35] A more sophisticated averaging procedure may have to be considered to complete the analysis. However, since our primary goal at this stage of the alloy work is to examine the nonlinear modifications to VCA introduced by CPA, we shall adopt the simple averaging procedure for $\overline{H}$.

VI. NUMERICAL RESULTS FOR THE ALLOYS

The CPA and VCA calculations have been carried out for the six III-V compound alloys listed in Table IV in the manner described in Sec. V. The table also contains the scattering strength, $\delta \equiv D_A - D_B$, for each alloy. As we are most interested in the difference between the CPA and the VCA results, we shall examine in detail the results for the alloy $Ga_xIn_{1-x}As$ which has the largest $|\delta|$ and, for comparison, another alloy $InAs_xSb_{1-x}$ with a smaller $|\delta|$. The results for the other alloys will be presented as needed.

TABLE IV. Semiconductor alloy systems A_xB_{1-x} studied in this work. The scattering strengths δ are in eV.

A	B	$\delta \equiv D_A - D_B$
GaP	GaAs	0.3562
GaP	InP	−0.5375
GaAs	InAs	−1.1125
GaSb	InSb	−0.0812
InP	InAs	−0.2188
InAs	InSb	−0.4937

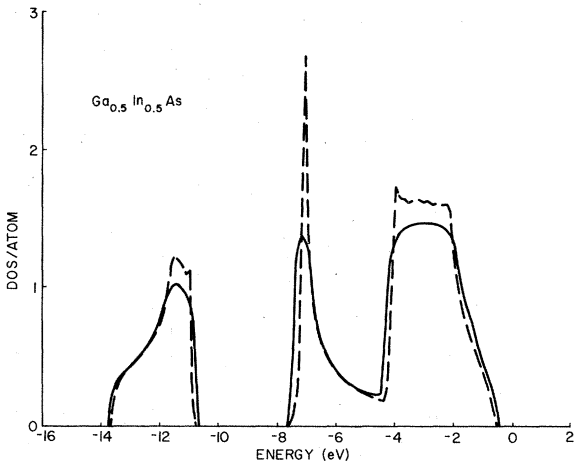

FIG. 4. Comparison between the densities of states resulting from VCA (the dashed curve) and CPA (the solid curve) for the $Ga_{0.5}In_{0.5}As$ alloy.

Figure 4 compares the CPA (the solid curves) and the VCA (the dashed curves) densities of states ρ for the alloy $Ga_{0.5}In_{0.5}As$. The CPA density of states merely represents a smeared version of that from VCA. The difference would be undetectable if both were broadened following the procedure used to compare the pure crystal densities to experiment in Figs. 3(a)–3(f). While they are not shown here, the ρ of $Ga_xIn_{1-x}As$ for $x = 0.1$, 0.3, 0.5, 0.7, and 0.9 have also been studied. In no cases did we find any unusual structures such as virtual bound states or impurity bands. The CPA density of states is even closer to the VCA result for the other alloys listed in Table IV because the scattering strengths in these cases are smaller. Until experimental resolutions are improved, it is clear that VCA and CPA are equally good for describing broadened spectra, like the photoemission energy distribution curves.

However, as mentioned before, there are more detailed features of the CPA results which are more interesting and can be tested by experiment. Below we shall examine the energy-level shifts, the related effective masses, and the scattering lifetimes. We have shown that these results provide a fundamental understanding[21] of the concentration variation of the E_0 gap and the lack of broadening in the measured E_0 spectra.[22,36-38] Since the basis for discussing these quantities are the self-energies $\sigma(E + i0) \equiv \eta(E) - i\gamma(E)$ and the function $F(E + i0) \equiv 4f(E + i0) = \mathrm{Re}F - i\pi\rho(E)$, where f is defined in Eq. (20) and $\rho(E)$ is the CPA density of states. We plot σ and F in Figs. 5 and 6, respectively, for $Ga_xIn_{1-x}As$ and $InAs_xSb_{1-x}$ with $x = 0.1$, 0.3, 0.5, 0.7, and 0.9.

Since the magnitude of γ, even in the strongest-scattering case $Ga_xIn_{1-x}As$, is small compared to

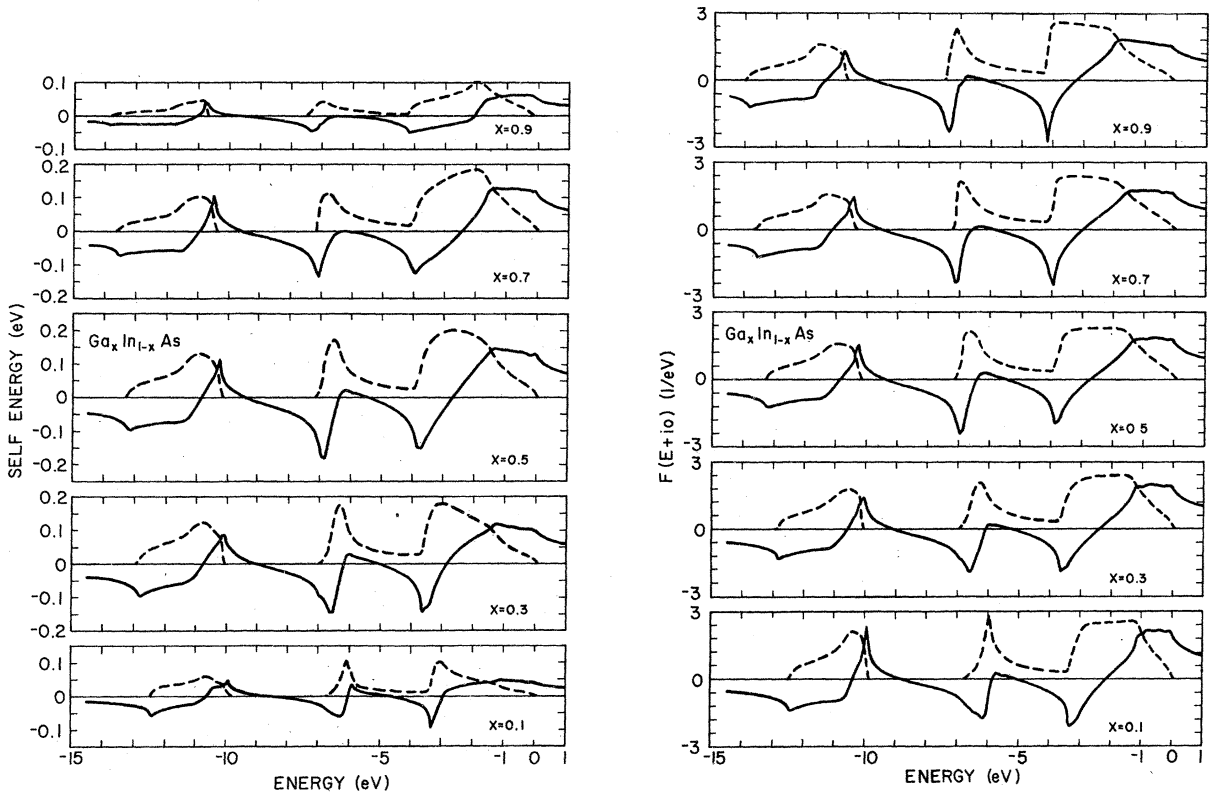

FIG. 5. Real part η (the solid curves) and the imaginary part γ (the dashed curves) of (a) the self-energy and (b) the F function defined in the text (ReF solid curve, $-\mathrm{Im}F = \pi\rho$ dashed curve) as a function of energy, for $Ga_xIn_{1-x}As$, with concentrations $x = 0.1$, 0.3, 0.5, 0.7, and 0.9. The zero of the abscissa is the energy at the top of the valence band of InAs.

the bandwidth, the usual relation among the CPA band energies E, the VCA band energies $\epsilon_n(\vec{k})$, and the real part of the self-energy $\eta(E)$ is valid,

$$E - \epsilon_n(\vec{k}) - \eta(E) = 0. \tag{21}$$

Figure 7 shows a comparison between the VCA bands (the solid curves) and the CPA bands (the dashed curves) for the $x = 0.5$ alloy. More quantitative examples of the energy changes are shown in Table V, where both the CPA and the VCA band energies at Γ, X, and L for $Ga_xIn_{1-x}As$ for five concentrations are listed. A general pattern can be observed: the higher energies of a subband are shifted upward while the lower energies move downward. This is a general feature of the CPA solution. This feature is clearly borne out in Fig. 5(a) where for each concentration the real part of σ, $\eta \equiv \mathrm{Re}\sigma$, is positive at the top of the band and negative at the lower end and varies in a systematic fashion in between. The energy shifts for the other alloys (e.g., see Fig. 6 for $InAs_xSb_{1-x}$) studied are qualitatively similar but are quantitatively smaller because they have smaller scattering strengths δ.

As mentioned before, our VCA energies are linear functions of x. The CPA energies are seen to deviate from the linear x dependence, but these deviations are different for different levels. We note that the solution to Eq. (21) with $\epsilon_n(\vec{k}) = \epsilon_{max}$, at the top of the VCA valence band yields the concentration dependence of the photoelectric threshold. This along with the variation of the E_0 gap has been discussed in detail elsewhere.[21]

Before passing onto other matters, we note that the variation of the effective mass at the valence-band edge is also easily determined from $\eta(E)$. Since our present empirical BOM band structure predicts effective masses that are too large,[16] a detailed analysis of the variation m^* with concentration is unwarranted. However, it is interesting nonetheless to examine how such an analysis proceeds and at least look at the trends it produces. The effective mass m^*_{VCA} at the top of the VCA bands along a given direction relates the energy variation $\delta\epsilon_n$ to an infinitesimal δk in that direction by $\delta\epsilon_n = -\hbar^2\delta k^2/2m^*_{VCA}$. The corresponding δE at the top energy E in CPA using Eq. (21) becomes $\delta E = -\hbar^2\delta k^2/[(1 - d\eta/dE)m^*_{VCA}]$, which implies the

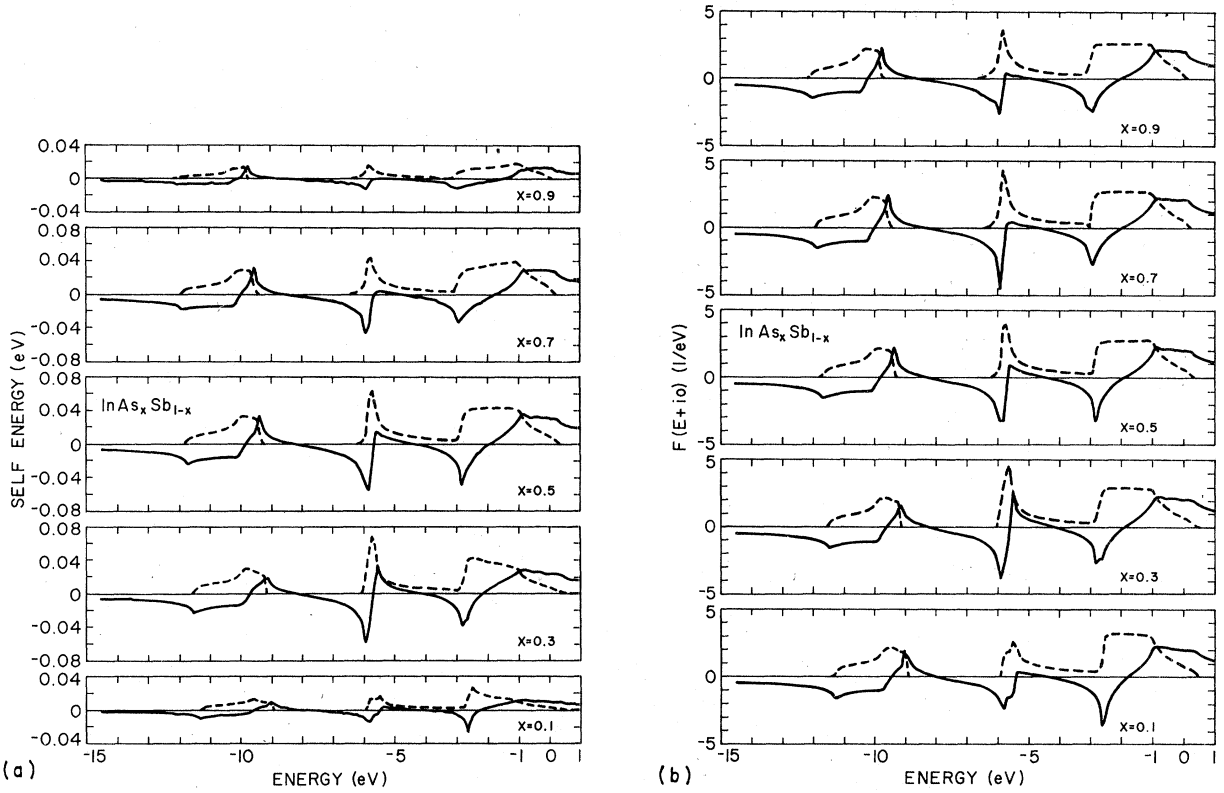

FIG. 6. Real part η (the solid curves) and the imaginary part γ (the dashed curves) of (a) the self-energy and (b) the F function defined in the text (ReF solid curve, $-\mathrm{Im}F=\pi\rho$ dashed curve) as a function of energy for $InAs_xSb_{1-x}$ with concentrations $x=0.1$, 0.3, 0.5, 0.7, and 0.9. The zero of the abscissa is the energy at the top of the valence band of InSb.

relation between the two masses:

$$m^*_{\mathrm{CPA}} = m^*_{\mathrm{VCA}}\left(1-\frac{d\eta}{dE}\right), \tag{22}$$

where $m^*_{\mathrm{VCA}}=[(x/m^*_A)+(y/m^*_B)]^{-1}$. Thus, the quantity $-d\eta/dE$ measures the differential ratio $(m^*_{\mathrm{CPA}}-m^*_{\mathrm{VCA}})/m^*_{\mathrm{VCA}}$, which from the numerical output is always positive at the Γ_{15} point for $Ga_xIn_{1-x}As$ alloys with values ranging from 1% to 5%. However, from the shape of the η curves in Fig. 5(a) just below the top of the valence band, it is evident that $d\eta/dE$ changes sign from $x=0.1$ to $x=0.9$. From the slopes of the straight-line portions of η one finds $-d\eta/dE=0.01$, 0.02, 0.05, 0.005, and -0.005, respectively, for $x=0.1$, 0.3, 0.5, 0.7, and 0.9. This behavior will influence hot-hole phenomena slightly. It is evident from Fig. 7, that for the $Ga_{0.5}In_{0.5}As$ alloy, m^*_{CPA} is larger than m^*_{VCA}, since the CPA bands have a lower curvature at the Γ_{15} point than the VCA bands.

As mentioned earlier, the alloy broadening γ is sensitive to energy (see Figs. 5 and 6). Table VI lists the γ values at the same energies listed in Table V for five $Ga_xIn_{1-x}As$ alloys. One interesting point to note is that γ for the Γ_{15} levels are quite small, consistent with the experimental finding[22,36-38] that alloying has very little effect on the broadening of the E_0 spectra. Previously, this lack of alloy broadening has been used as evidence against the existence of any alloy disorder[23] contribution to the observed nonlinear

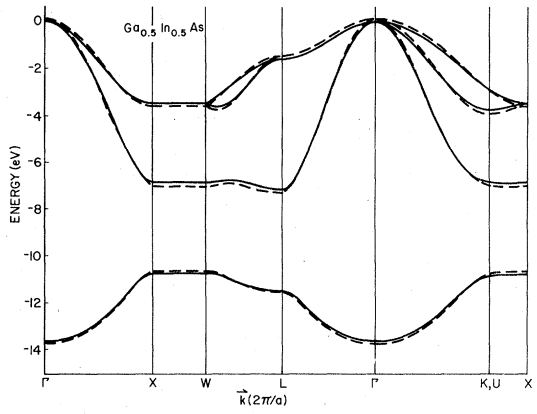

FIG. 7. Comparison of the band structures of $Ga_{0.5}In_{0.5}As$ calculated from VCA (the solid curves) and from CPA (the dashed curves) as given by Eq. (21).

TABLE V. Comparison between the CPA valence-band energies (the E defined in Eq. 21) and the corresponding VCA values at the symmetry points for five $Ga_xIn_{1-x}As$ alloys. The first number for each state is the CPA result and the second number is the VCA result. All the energies are in eV with respect to the top of the valence band (Γ_{15}) of the pure InAs compound.

Concentration (x)	0.1	0.3	0.5	0.7	0.9
Γ_{15}	0.007	0.034	0.021	−0.024	−0.121
	−0.020	−0.060	−0.100	−0.140	−0.180
Γ_1	−12.443	−12.865	−13.239	−13.597	−13.935
	−12.389	−12.769	−13.100	−13.530	−13.910
X_5	−2.913	−3.235	−3.514	−3.744	−3.925
	−2.920	−3.166	−3.400	−3.640	−3.880
X_3	−5.939	−6.397	−6.816	−7.116	−7.375
	−5.970	−6.310	−6.650	−6.990	−7.330
X_1	−9.956	−10.117	−10.290	−10.504	−10.760
	−10.000	−10.200	−10.400	−10.600	−10.800
L_3	−1.072	−1.274	−1.460	−1.751	−2.084
	−1.162	−1.360	−1.600	−1.840	−1.080
L_2	−6.676	−6.896	−7.075	−7.178	−7.221
	−6.632	−6.793	−6.934	−7.065	−7.179
L_1	−10.590	−10.863	−11.159	−11.447	−11.716
	−10.598	−10.847	−11.113	−11.395	−11.691

concentration dependence of E_0. These results demonstrate that such an argument is unjustified.

While even the largest width γ at the Γ_{15} point is small compared to the resolution of optical experiments (including modulation spectroscopy) it does reach a value of $\gamma = 0.008$ eV for the $Ga_{0.5}In_{0.5}As$ alloy. The width is related to the mean time between collisions τ by the equation $\tau = \hbar/2\gamma$. Thus, in this case $\tau \cong 4\times10^{-14}$ sec, which is quite short. For states deep in the valence bands, γ can be as large as 0.2 eV corresponding to a $\tau \approx 10^{-15}$ sec. Although the scattering lifetime τ, strictly speaking, is not the same as the momentum transfer time τ_m that appears in the mobility calculation, they are closely related. In view of such a large τ, it is unlikely that hot holes will have a large mobility in concentrated $Ga_xIn_{1-x}As$ alloys.

The energy dependences of both η and γ discussed above can be qualitatively understood from the CPA equation [Eq. (19)]. A lower-order approximation to σ can be obtained by substituting $\sigma = 0$ on the right-hand side of the equation. Then the solution is

$$\sigma = xy\delta^2 f(z-\sigma)\,. \tag{23}$$

An alternative expression to Eq. (20) for $f(E-\sigma)$ can be written in the form[4]

$$f(E-\sigma) = \frac{1}{4}\int dE'\,\frac{\rho(E')}{E+i0-E'}\,, \tag{24}$$

where $\rho(E)$ is the CPA density of states. It is easy to see that the $\mathrm{Re}f(E-\sigma)$ is always positive at the top of the valence band and always negative at the bottom. It is also evident that the $\mathrm{Im}f(E-\sigma) = -\frac{1}{4}\pi\rho(E)$ is zero outside the CPA-broadened band. If the same argument is applied to the conduction band, then it will shift, because of disorder, down toward the valence band. Hence, as we have already concluded from prior arguments, disorder tends to narrow the band gap.[21]

While the lower-order approximation in Eq. (23) is qualitatively correct in relating σ to F and, in particular, yields the correct sign of η and the smallness of γ at the band top, no detailed agreement between the shapes of ρ and γ should be expected for the scattering strengths in the III-V compound alloys. A comparison between Figs. 5(a) and 5(b) and between 6(a) and 6(b) shows that for $x = 0.5$ the shapes of the curves for σ and F are remarkably similar, but they have marked

TABLE VI. Imaginary part of the self-energy (in eV), $\gamma \equiv \mathrm{Im}\sigma(E+i0)$, at the CPA band energies listed in Table V for five $Ga_xIn_{1-x}As$ alloys.

Concentration (x)	0.1	0.3	0.5	0.7	0.9
Γ_{15}	0.002	0.005	0.008	0.007	0.004
Γ_1	0.004	0.007	0.005	0.004	0.001
X_5	0.094	0.173	0.155	0.101	0.034
X_3	0.074	0.169	0.127	0.038	0.012
X_1	0.011	0.038	0.051	0.052	0.037
L_3	0.027	0.086	0.145	0.179	0.095
L_2	0.006	0.013	0.014	0.009	0.028
L_1	0.061	0.121	0.123	0.087	0.030

differences for the lower concentrations. For $Ga_xIn_{1-x}As$ in Fig. (5), while the peaks of $\rho(E)$ for the top band shift from higher to lower energy as x increases the corresponding peaks of γ shift in the other direction. Similar variations of the peak positions of γ are also found in Fig. (6) for $InAs_xSb_{1-x}$. Although the density-of-states curves show no evidence of virtual bound states, the γ curves display precursors to such features for the low-concentration alloys. The peak of γ at $x=0.1$ for $Ga_xIn_{1-x}As$ (GaAs as an impurity in InAs) is around 3 eV, which is a remnant of the center of the peak position of the GaAs density of states [see Fig. 3(b)]. Similarly, the peak of γ at 2 eV for $Ga_{0.9}In_{0.1}As$ (InAs as the impurity) coincides with center of the peak position of the pure InAs density of states [see Fig. 3(e)]. Similar findings also apply to $InAs_xSb_{1-x}$ alloys.

These features can be understood, along with some others, in terms of the following physical model. For moderate scattering strengths (well away from the split band limit), $\gamma(E)$ tends to be large in energy regions where two conditions are satisfied: (a) there is overlap between the densities of states $\rho_A(E)$ and $\rho_B(E)$ of the pure constituents, and (b) the alloy density of states $\rho(E)$ is large. The first condition arises because resonant scattering (or a large amount of state mixing) can occur. The second condition enters because in that case there is a large density of final states into which scattering can take place. Now it is easier to understand the shape of the $\gamma(E)$ curves. Near the band edges, $\rho(E)$ goes to zero; hence, $\gamma(E)$ also is small there. In the GaInAs alloy, the GaAs valence bands are generally at lower energies than the corresponding bands in InAs (see Table IV). Focus attention on the uppermost large feature in $\gamma(E)$ in Fig. 5 at the various concentrations. On the InAs-rich side ($x=0.1$) this feature peaks around -3 eV. This is because the GaAs as an impurity in InAs has states in this region which strongly scatter the holes. At the other end of the concentration range ($x=0.9$), where the InAs is the impurity in GaAs, the peak of γ is at a higher energy ~ -2 eV. An important consequence of this shift in the peak of γ is that alloy scattering is stronger near the top of the valence band in the GaAs-rich side than in the opposite case. For example, at -1 eV, the self-energies are $\gamma \cong 0.1$ eV for $x=0.9$ but only ~ 0.005 eV for $x=0.1$. This should have important consequences on hot-hole phenomena. Based on these arguments, we can speculate about the trends that will be found when the conduction-band calculation is done. GaAs has a much larger band gap than InAs. Thus, while the GaAs levels in the valence band are at lower energies than those of InAs, the reverse will be true in the conduction bands. Hence, once again impurity scattering near the conduction-band edge should be stronger on the GaAs-rich side.

Thus, while there are similarities between $\pi\rho$ and γ in all the alloys, they never have exactly the same shape as can be seen from Figs. 5 and 6. Hence, it is essential to use the complete CPA Eq. (19) rather than the approximate expression Eq. (23) if details are to be given properly. This reemphasizes the need for using CPA rather than VCA since Eq. (23) is, after all, an improvement over the lowest-order correction to VCA,[39] and it is still inadequate.

VII. SUMMARY AND DISCUSSION

There are two major subdivisions to this work: the critical reexamination of BOM as it applies to band structures, and the CPA calculation of the properties of the III-V compound alloys from BOM. There are two reasons for using BOM. First, BOM provides a physical picture of the bonding in zinc-blende compounds. Second, the model effectively identifies the important alloy disorder parameters which it turns out can be incorporated into the framework of CPA.

However, BOM has intrinsic defects which prevent it from attaining high accuracy for all features of the band structures. It does not predict the correct effective masses nor the correct energy dispersion along Z or Σ axis. Moreover, we found that this lack of dispersion along the Z axis cannot be remedied either by including the third-nearest bond interactions nor by including the antibounding basis functions (see Appendix B). Based on the conclusions of Chadi,[40] the inclusion of some d-state character into the basis set, and an explicit accounting of the nonorthogonality of the basis functions may remedy these faults. However, we note that the usual linear-combination-of-atomic-orbitals (LCAO) results[26] show that this dispersion along Z exists if the matrix elements, in the terminology of Slater and Koster,[41] like $E_x(110)$ and $E_x(011)$ are different and are included. Since the bond bases (including the antibonding state) and the LCAO bases are related to each other by a unitary transformation, the two descriptions should be completely equivalent. The LCAO matrix elements $E_x(110)$ and $E_x(011)$ in terms of the bond bases involve the second-, third-, and fourth-nearest bond interactions. To understand the cause of the defects in BOM, the symmetry of the matrix elements and the higher-order terms have to be carefully reexamined. Despite these problems, the broadened density of states based on the present BOM fit the gross

features of the experimental spectra reasonably well. Therefore, one expects the BOM parameters derived by fitting this data to be at least qualitatively correct.

A calculation based on the "single-bond" CPA is shown to be easily implemented. The only BZ integration needed is the calculation of the VCA density of states, and this can be effectively carried out using the new BZ integration method.[9] While the CPA and the VCA densities of states differ, the differences in the alloys studied would be difficult to resolve experimentally at present. The more useful CPA results involve detailed features such as band-level shifts, effective masses, scattering lifetimes, etc.

While the explicit results found for the six III-V compound alloys are informative, the most important consequence of this study is the development of the procedures to obtain detailed information about semiconductor alloys using CPA. Moreover, when it is improved as suggested below, the theory will be sufficiently broad to encompass the full range of experiments conducted on these materials. Then it will be possible to interrelate the results of many experiments through a single formalism. The improvements and extensions needed to make this a quantitative method include: (i) improvement of the pure constituent's band structures by including (a) the conduction bands, (b) the spin-orbit interactions,[26,42] and (c) some d-state character and nonorthogonality in the basis set[40]; (ii) a systematic study of the best parametrization method[42] with emphasis placed on isolating the important variations from one compound to another; (iii) incorporation of alloy potential renormalizations to account for charge shifts and lattice-constant changes[7]; (iv) examination of the need to treat the off-diagonal elements in a cluster CPA[31,33,34]; (v) calculation of the transport properties,[43,44] e.g., the mobility, the frequency-dependent dielectric constant, etc. While a good start has been made, it is fairly obvious that much remains to be done in this field.

ACKNOWLEDGMENTS

This work was supported in part by NSF and NASA.

APPENDIX A

The matrix elements $H_{\alpha\alpha'} \equiv \langle \vec{k}\alpha | H_0 | \vec{k}\alpha' \rangle$ for the BOM described in Sec. I are listed below. The symbols x, y, and z stand for $\frac{1}{4}k_x a$, $\frac{1}{4}kya$, and $\frac{1}{4}k_z a$, respectively.

$$H_{11} = D + 2D_2[\cos(2x+2y)+\cos(2x+2z)+\cos(2z+2y)] + 2D_3[\cos(2x-2y)+\cos(2y-2z)+\cos(2x-2z)] ,$$

$$H_{22} = D + 2D_2[\cos(2x+2y)+\cos(2y-2z)+\cos(2x-2z)] + 2D_3[\cos(2x-2y)+\cos(2y+2z)+\cos(2x+2z)] ,$$

$$H_{33} = D + 2D_2[\cos(2x-2y)+\cos(2y-2z)+\cos(2x+2z)] + 2D_3[\cos(2x+2y)+\cos(2y+2z)+\cos(2x-2z)] ,$$

$$H_{44} = D + 2D_2[\cos(2x-2y)+\cos(2y+2z)+\cos(2x-2z)] + 2D_3[\cos(2x+2y)+\cos(2y-2z)+\cos(2x+2z)] ,$$

$$\begin{aligned} H_{12} = {} & 2\{\gamma_1^s \cos(x+y) + 2\gamma_2 \cos(x-y)\cos 2z + \gamma_3^s[\cos(3x+y+2z)+\cos(3x-y)+\cos(3x+3y)+\cos(x+3y-2z) \\ & +\cos(3x+y-2z)+\cos(x+3y+2z)+\cos(3y-x)]\} \\ & -2i\{\gamma_1^a \sin(x+y) - \gamma_3^a[\sin(3x+y+2z)+\sin(3y-z)+\sin(3x+3y)+\sin(x+3y-2z)+\sin(3x+y-2z) \\ & +\sin(x+3y+2z)+\sin(3y-x)]\} , \end{aligned}$$

$$\begin{aligned} H_{13} = {} & 2\{\gamma_1^s \cos(x+z) + 2\gamma_2 \cos(x-z)\cos 2y + \gamma_3^s[\cos(3x+3z)+\cos(3x-2y+z) \\ & +\cos(x-2y+3z)+\cos(3x+2y+z) \\ & +\cos(3x-z)+\cos(x+2y+3z)+\cos(3z-x)]\} \\ & -2i\{\gamma_1^a \sin(x+z) - \gamma_3^a[\sin(3x+3z)+\sin(3x-2y+z) \\ & +\sin(x-2y+3z)+\sin(3x+2y+z)+\sin(3x-z)+\sin(x+2y+3z)+\sin(3z-x)]\} , \end{aligned}$$

$$\begin{aligned} H_{14} = {} & 2\{\gamma_1^s \cos(y+z) + 2\gamma_2 \cos 2x \cos(y-z) + \gamma_3^s[\cos(2x+y+3z)+\cos(3z-y)+\cos(2x+3y+z)+\cos(3y-z) \\ & +\cos(3z+y-2x)+\cos(3y+3z)+\cos(3y+z-2x)]\} \\ & -2i\{\gamma_1^a \sin(y+z) - \gamma_3^a[\sin(2x+y+3z)+\sin(3z-y)+\sin(2x+3y+z)+\sin(3y-z)+\sin(y+3z-2x) \\ & +\sin(3y+3z)+\sin(3y+z-2x)]\} , \end{aligned}$$

$$H_{23}=2\{\gamma_1^s\cos(y-z)+2\gamma_2\cos2x\cos(y+z)+\gamma_3^s[\cos(z-3y-2x)+\cos(3y+z)+\cos(3z-3y)+\cos(2x-y+3z)+\cos(2x-3y+z)+\cos(3z-2x-y)+\cos(3z+y)]\}$$
$$+2i\{\gamma_1^a\sin(y-z)+\gamma_3^a[\sin(z-2x-3y)-\sin(3y+z)+\sin(3z-3y)+\sin(2x+3z-y)+\sin(2x-3y+z)+\sin(3z-2x-y)+\sin(3z+y)]\}\ ,$$
$$H_{24}=2\{\gamma_1^s\cos(x-z)+2\gamma_2\cos2y\cos(x+z)+\gamma_3^s[\cos(z-3x-2y)+\cos(3x+z)+\cos(3z-x-2y)+\cos(x+3z)+\cos(2y+z-3x)+\cos(3z-3x)+\cos(2y+3z-x)]\}$$
$$+2i\{\gamma_1^a\sin(x-z)+\gamma_3^a[\sin(z-3x-2y)-\sin(3x+z)+\sin(3z-x-2y)+\sin(x+3z)+\sin(2y+z-3x)+\sin(3z-3x)+\sin(2y+3z-x)]\}\ ,$$
$$H_{34}=2\{\gamma_1^s\cos(x-y)+2\gamma_2\cos2z\cos(x+y)+\gamma_3^s[\cos(3x+y)+\cos(y-3x-2z)+\cos(x+3y)+\cos(3y-x-2z)+\cos(3y-x+2z)+\cos(2z-3x+y)+\cos(3y-3x)]\}$$
$$+2i\{\gamma_1^a\sin(x-y)+\gamma_3^a[\sin(y-3x-2z)-\sin(3x+y)+\sin(x+3y)+\sin(3y-x-2z)+\sin(3y-x+2z)+\sin(2z-3x+y)+\sin(3y-3x)]\}$$

We note that, except for the additional terms involving γ_3^s and γ_3^a, the above results appear in the appendix of Ref. 15. There the indices 2 and 3 are interchanged. It turns out that these additional terms do not affect the relations between the band energies and the Block matrix elements along the [100] and [111] directions. These relations (in the twofold degenerate case) for the Δ axis are

$$\Delta_5=H_{11}-H_{14}\ ,\quad \Delta_{2',1}=H_{11}+H_{14}\pm2|H_{12}|\ ,$$

and for the Λ axis are

$$\Lambda_3=H_{22}-H_{23}\ ,$$
$$\Lambda_{1,1}=\tfrac{1}{2}\{H_{11}+H_{22}+2H_{23}\pm[(H_{11}-H_{22}-2H_{23})^2+12|H_{12}|^2]^{1/2}\}\ .$$

The explicit expressions for the energies for these two axes are

$$\Delta_5=D+2D_2+2D_3-2\gamma_1^s-6\gamma_3^s+4(D_2+D_3+\gamma_2+2\gamma_3^s)\cos2x\ , \tag{A1}$$
$$\Delta_{2',1}=D+2D_2+2D_3+2\gamma_1^s+6\gamma_3^s+4(D_2+D_3+\gamma_2+2\gamma_3^s)\cos2x\pm\{[(2\gamma_1^s+4\gamma_2+6\gamma_3^s)\cos x+8\gamma_3^s\cos3x]^2+[(2\gamma_1^a-2\gamma_3^a)\sin x-8\gamma_3^s\sin3x]^2\}^{1/2} \tag{A2}$$
$$\Lambda_3=D+4D_2+2D_3-2\gamma_1^s-2\gamma_2-6\gamma_3^s+(2D_2+4D_3-2\gamma_2-8\gamma_3^s)\cos4x\ , \tag{A3}$$
$$\Lambda_{1,1}=D+2D_2+4D_3+2\gamma_1^s+2\gamma_2+6\gamma_3^s+(4D_2+2D_3+2\gamma_2+8\gamma_3^s)\cos4x\pm\{4[D_2-D_3+\gamma_1^s+\gamma_2+3\gamma_3^s-(D_2-D_3-\gamma_2+4\gamma_3^s)\cos4x]^2+12[(\gamma_1^s+2\gamma_2+4\gamma_3^s)\cos2x+3\gamma_3^s\cos6x]^2+12[(\gamma_1^a-4\gamma_3^a)\sin2x-3\gamma_3^a\sin6x]^2\}^{1/2}\ . \tag{A4}$$

APPENDIX B

Here we show that there is no dispersion of the BOM bands along the Z axis even with the whole set of parameters in Sec. II included. We start with the H matrix at the symmetry point X in terms of the four Bloch bases $|X1\rangle$, $|X2\rangle$, $|X3\rangle$, and $|X4\rangle$:

$$H_X=\begin{bmatrix} h & is & is & -r \\ -is & h & -r & -is \\ -is & -r & h & -is \\ -r & is & is & h \end{bmatrix}, \tag{B1}$$

where

$$h\equiv D-2D_2-2D_3\ ,$$
$$r\equiv-2\gamma_1^s+4\gamma_2+2\gamma_3^s\ ,$$

and

$$s\equiv-2\gamma_1^a-6\gamma_3^a\ .$$

Let us define a unitary transformation which transforms the set $\{|X\alpha\rangle,\alpha=1,4\}$ into a new set:

$$|Z1\rangle\equiv|X1\rangle\ ,$$
$$|Z2\rangle\equiv\cos y\,|X2\rangle-\sin y\,|X4\rangle\ ,$$
$$|Z3\rangle\equiv|X3\rangle\ ,$$

and

$$|Z4\rangle\equiv\sin y\,|X2\rangle+\cos y\,|X4\rangle\ .$$

This transformation changes the matrix H_X into

$$H_z = \begin{bmatrix} h & r\sin y + is\cos y & is & -r\cos y + is\sin y \\ r\sin y - is\cos y & h & -r\cos y - is\sin y & -is \\ -is & -r\cos y + is\sin y & h & -r\cos y - is\sin y \\ r\cos y - is\sin y & is & -r\cos y + is\sin y & h \end{bmatrix}, \tag{B2}$$

This matrix can be shown to be identical to the Hamiltonian matrix at $\vec{k}=(1,k_y,0)(2\pi/a)$ along Z with k_y related to y by $y=\frac{1}{4}k_y a$. Thus, the eigenvalues of H_Z are identical to those of H_X and there is no dispersion, i.e., $E(\vec{k})$ is a constant, along the Z axis.

The above argument can be extended to include the antibonding orbitals. In that case, the H_x and H_Z are 8×8 matrices having the form:

$$\begin{pmatrix} H_C & H_{CV} \\ H_{VC} & H_V \end{pmatrix}$$

where H_C, H_{CV}, and H_V are 4×4 matrices having similar forms to (B1) and (B2). Thus, H_X and H_Z can be transformed into each other by a similar unitary transform. Once again, there is no dispersion along the Z axis.

[1]There are many books on the electronic structure of semiconductors. Good examples are: the series *Semiconductors and Semimetals* edited by R. Willardson and A. Beer (Academic, New York, 1966–1979); M. Cardona, Solid State Phys. Suppl. 11 (1969). A detailed comparison of the more recent data with band-structure results can be found in Ref. 2.

[2]J. R. Chelikowsky and M. L. Cohen, Phys. Rev. B 14, 556 (1976).

[3]Paul Soven, Phys. Rev. 156, 809 (1967).

[4]B. Velicky, S. Kirkpatrick, and H. Ehrenreich, Phys. Rev. 175, 747 (1968).

[5]For extensive reviews see: H. Ehrenreich and L. M. Schwartz, Solid State Phys. 31, 149 (1976); J. Elliot, J. A. Krumhansl, and P. S. Leath, Rev. Mod. Phys. 45, 4651 (1974).

[6]L. Nordheim, Ann. Phys. (Paris) 9, 607; 9, 641 (1931).

[7]J. A. Van Vechten and T. K. Bergstresser, Phys. Rev. B 1, 3351 (1970).

[8]J. R. Hauser, M. A. Littlejohn, and T. H. Glisson, Appl. Phys. Lett. 28, 458 (1976).

[9]D. Stroud and H. Ehrenreich, Phys. Rev. B 2, 3197 (1970).

[10]A.-B. Chen, Phys. Rev. B 16, 3291 (1977).

[11]Recently, B. L. Gyorffy and G. M. Stocks and their co-workers have carried out CPA muffin-tin calculations for NiCu and NbMo alloys, [see Bull. Am. Phys. Soc. 22, 348 (1977) and Proceedings of the International Conference on Physics of Transition Metals, University of Toronto, Canada (unpublished)].

[12]J. S. Faulkner, Phys. Rev. B 13, 2391 (1976).

[13]D. W. Taylor, in *Proceedings of the Michigan State University Summer School on Alloys*, edited by W. M. Hartmann, P. A. Schroeder, and C. L. Foiles MSU, East Lansing, Mi., 1972), p. 103 and references therein.

[14]A. Gonis and J. W. Garland, Phys. Rev. B 16, 2424 (1977) and references therein.

[15]W. A. Harrison, Phys. Rev. B 8, 4487 (1973); W. A. Harrison and S. Ciraci, *ibid.* 10, 1516 (1974).

[16]P. T. Pantelides and W. A. Harrison, Phys. Rev. B 11, 3006 (1975).

[17]N. J. Shevchik, J. Tejeda, and M. Cardona, Phys. Rev. B 9, 2627 (1974).

[18]D. Stocker, Proc. R. Soc. Lond. 270, 397 (1962).

[19]L. Ley, R. A. Pollak, F. R. McFeely, S. P. Kowalczyk, and A. Shirley, Phys. Rev. B 9, 600 (1973).

[20]A.-B. Chen, Phys. Rev. B 7, 2230 (1973).

[21]A.-B. Chen and A. Sher, Phys. Rev. Lett. 40, 900 (1978).

[22]Experimental bowing parameters and references are summarized in Refs. 7 and 23.

[23]R. Hill, J. Phys. C 7, 521 (1974).

[24]C. Huang, J. A. Moriarty, A. Sher, and R. A. Breckenridge, Phys. Rev. B 12, 5395 (1975); C. Huang, J. A. Moriarty, and A. Sher, *ibid.* 14, 2539 (1976).

[25]S. T. Pantelides, Phys. Rev. B 11, 5082 (1975).

[26]D. J. Chadi and M. L. Cohen, Phys. Status Solidi B 68, 405 (1975).

[27]A.-B. Chen and B. Segall, Phys. Rev. B 12, 600 (1975).

[28]D. E. Eastman, W. D. Grobman, J. L. Freeouf, and M. Erbudak, Phys. Rev. B 9, 3473 (1974).

[29]The values of the thresholds in Table II are obtained from Table II of Ref. 17.

[30]Previous experimental thresholds (in eV) are: GaAs (5.47), GaSb (4.76), InAs (5.31), InSb (4.77), G. W. Gobeli and F. G. Allen, Phys. Rev. 137, A248 (1965); InP (5.69), T. E. Fischer, Phys. Rev. 139, A1228 (1965).

[31]J. A. Blackman, D. M. Esterling, and N. T. Berk, Phys. Rev. B 4, 2412 (1971).

[32]H. Fukuyama, H. Krankauer, and L. Schwartz, Phys. Rev. B 10, 1173 (1974).

[33]H. C. Hwang and A. Sher, Phys. Rev. B 12, 5514 (1975); H. C. Hwang, R. A. Breckenridge, and A. Sher, *ibid.* 16, 3840 (1977).

[34]T. Wolfram and J. Callaway, Phys. Rev. 130, 2207 (1963).

[35]It was pointed out that some matrix elements for semiconductors in LCAO can be scaled according to the inverse square of the bond lengths; see, W. A. Harrison, Proceedings of the German Physical Society Munster, 1977 (unpublished).

[36]E. W. Williams and V. Rehn, Phys. Rev. 172, 798 (1968).
[37]C. Abibert, G. Bordee, A. Laigier, and J. Chevallier, Phys. Rev. B 6, 1301 (1972).
[38]S. Vishnubhatla, B. Eyglvnent, and J. Woolly, Can. J. Phys. 47, 1611 (1969).
[39]Equation (23) yields the lowest-order correction to VCA if the σ in $f(\varepsilon-\sigma)$ on the right-hand side is set equal to zero.
[40]D. J. Chadi, Phys. Rev. B 16, 3572 (1977).
[41]J. C. Slater and G. F. Koster, Phys. Rev. 94, 1498 (1954).
[42]G. Dresselhaus and M. S. Dresselhaus, Phys. Rev. 160, 649 (1967).
[43]B. Velicky, Phys. Rev. 184, 416 (1969).
[44]A.-B. Chen, G. Weisz, and A. Sher, Phys. Rev. B 5, 2897 (1972).